Please do not adjust margins

Journal Name

ARTICLE

Development, characterisation and *in vitro* evaluation of lanthanide-based FPR2/ALX-targeted imaging probes

Received 00th January 20xx,
Accepted 00th January 20xx

DOI: 10.1039/x0xx00000x

www.rsc.org/

Tamara Boltersdorf[a], Junaid Ansari[b], Elena Y. Senchenkova[b], Lijun Jiang[a], Michael Coogan[c], Felicity N. E. Gavins[b,d*], Nicholas J. Long[a,*]

We report the design, preparation and characterisation of three small-molecule, Formyl Peptide Receptor (FPR)-targeted lanthanide complexes (Tb.**14**, Eu.**14** and Gd.**14**). Long-lived, metal-based emission was observed from the terbium complex (τ_{H2O} = 1.9 ms), whereas only negligible lanthanide signals were detected in the europium analogue. Ligand-centred emission was investigated using Gd.**14** at room temperature and 77 K, leading to the postulation that metal emission may be sensitised via a ligand-based charge transfer state of the targeting Quin C1 unit. Comparatively high longitudinal relaxivity values (r_1) for octadentate metal complexes of Gd.**14** were determined (6.9 $mM^{-1}s^{-1}$ at 400 MHz and 294 K), which could be a result of a relative increase in twisted square antiprism (TSAP) isomer prevalence compared to typical DOTA constructs (as evidenced by NMR spectroscopy). *In vitro* validation of concentration responses of Tb.**14** via three key neutrophil functional assays demonstrated that the inflammatory responses of neutrophils (i.e. chemotaxis, transmigration and granular release) remained unchanged in the presence of the compound. Using a time-resolved microscopy set-up we were able to observe binding of the Tb.**14** probe to stimulated human neutrophils around the cell periphery, while in the same experiment with un-activated neutrophils, no metal-based signals were detected. Our results demonstrate the utility of Tb.**14** for time-resolved microscopy with lifetimes several orders of magnitude longer than autofluorescent signals and a preferential uptake in stimulated neutrophils.

Introduction

The inflammatory response is implicated in the progression of a variety of disease states including Alzheimer's Disease,[1] stroke,[2] sickle cell disease[3] and cancer[4] and often the extent of inflammation is a key factor controlling disease prognosis. As a result, there is interest in gaining mechanistic insights into the physiological processes underlying inflammation in order to address clinical issues and provide screening tools for drug discovery programmes.[5]

The Formyl Peptide Receptor (FPR) family[6] comprising FPR1, FPR2/ALX (also known as the lipoxin A_4 receptor, and previously termed FPR-like 1 [FPRL1, but not to be confused with FPR1, nomenclature detailed in reference[6]]) and FPR3 (also known as FPRL2) in humans are categorised as G-protein coupled receptors (GPCR) and have attracted interest as a result of their role in modulating both pro- and anti-inflammatory pathways[7,8,9] during all phases of the inflammatory response (including initiation, chemotactic signaling, propagation, resolution and tissue repair). Amongst these, FPR1 and FPR2/ALX are expressed on the cell surface of human neutrophils and can induce chemotaxis, mobilise adhesion molecules and inhibit migration of these immune cells.[6] Although these receptors are also known to be upregulated in a variety of disease conditions,[10] the understanding of their specific physiological functions still remains limited, creating a need to prepare probes that enable their roles to be studied in a biological context.[11,7]

Compounds to enable targeting of FPR1 and FPR2/ALX to track neutrophils in inflammatory conditions have been previously reported as imaging agents for example, in magnetic resonance imaging (MRI),[12] positron emission tomography (PET),[13] optical[14] and single-photon emission computed tomography (SPECT).[15,16] These constructs, however, have been derived from the peptide-based FPR1 antagonist cinnamoyl-F-(D)L-F-(D)L-F (cFLFLF), which is highly hydrophobic and often results in poor target to background ratios, necessitating incorporation of, for instance, large PEGylated chains.[17] Another strategy reports synthetic modifications of the potent, peptide-based FPR agonist formyl-Met-Leu-Phe (fMLF) to prepare agents for both optical- and radio-imaging of FPRs.[18,19,20] These compounds, however, are unselective for receptor subtype (FPR1 or FPR2/ALX) and the known high potency of the modified agonist ligand fMLF results in a risk of unwanted receptor activation,[6] possibly even causing an inflammatory response when using the system for imaging.

[a] *Department of Chemistry, Imperial College London, Molecular Sciences Research Hub, White City, London, W12 0BZ, UK.*
[b] *Department of Molecular & Cellular Physiology, Louisiana State University Health Sciences Center-Shreveport, Shreveport, LA, 71130, USA.*
[c] *Department of Chemistry, Lancaster University, Lancaster, LA1 4YB, UK*
[d] *Department of Life Sciences, Brunel University London, Uxbridge, Middlesex, UB8 3PH, UK.*

Electronic Supplementary Information (ESI) available including crystallographic data and supplementary figures. See DOI: 10.1039/x0xx00000x

This journal is © The Royal Society of Chemistry 20xx

Please do not adjust margins

Please do not adjust margins

To circumvent the issues encountered with peptide systems, small-molecule, FPR-specific ligands that are synthetically and metabolically more robust, as well as cheaper to prepare and modify,[21] could provide a convenient alternative. Large-scale screening for such binding motifs have been previously performed, and a non-peptidic, mild FPR2/ALX agonist, 4-butoxy-N-[2-(4-methoxy-phenyl)-4-oxo-1,4-dihydro-2H-quinazolin-3-yl]-benzamide (Quin C1),[22] was identified in 2004. The compound was assessed for its concentration dependence *in vitro,* and *in vivo* properties were evaluated,[22,23] but to our knowledge it has not been derivatised to form an imaging agent for FPR2/ALX.

Fluorescence microscopy is a widely used technique for cellular imaging and pre-clinical models that surpasses many other modalities in terms of sensitivity and spatial resolution, allowing systems to be investigated on a cellular and subcellular level.[24] Although numerous targeted and fluorescent probes have been designed to enable visualisation of surface receptors by fluorescence microscopy, these are often accompanied with various drawbacks.[25] Amongst these are poor photostability, difficulty in separating signals from autofluorescence, large probe sizes, as well as sometimes restricted labelling sites when dealing with peptide-based targeting groups.[26,27]

Time-resolved microscopy relies on detection of the luminescence lifetimes of a sample, which are not substantially affected by photobleaching events. In addition, if a sufficiently long-lived probe is used, this can create signal differences of several orders of magnitude between compound and cellular background, allowing for a much more accurate picture of the agent within a cell.[28,29] For example, long-lived iridium probes have been developed to image cancer cells[30,31] and for uses in live zebrafish.[32,33]

Stable lanthanide(III) chelates based on terbium or europium often have highly desirable properties for cellular imaging: their emission is long-lived (up to ms range), the separation between excitation and emission bands is large and metal-based emission is characterised by sharp, distinctive peaks that are only minimally altered by different ligand surroundings.[34,35,36,37] Recently, the first and, to the best of our knowledge, only example of time-resolved FPR2/ALX imaging in cells has been reported using an iridium complex coupled to a peptidic FPR2/ALX agonist.[38] However, the probe was designed based on a potent FPR2/ALX agonist and caused a dose-dependent response in human umbilical vein endothelial cells (HUVECs), altering cellular properties and rendering it not ideal as an imaging agent.[38]

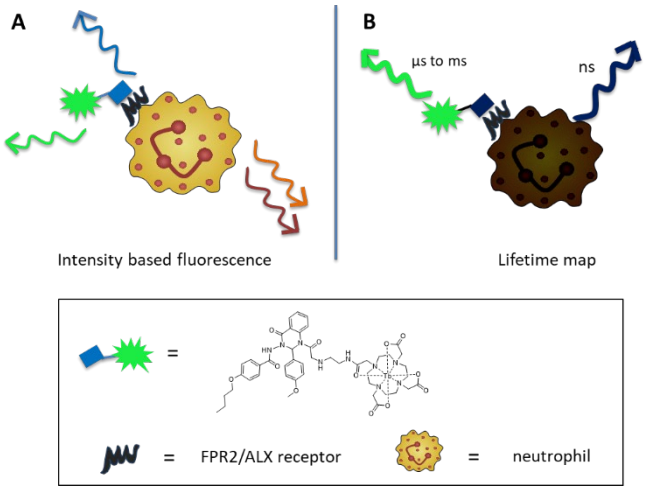

Figure 1: Schematic illustrating A) the multiple emission sources occuring in intensity-based luminescence measurements (from organic probe component, metal, and diverse autofluorescent sources within a neutrophil) and B) the possibility to separate metal-based lifetime (µs to ms scale) from all other signals (ns scale).

Therefore, by combining the small-molecule targeting group Quin C1 with a stable Tb(III) chelate, we aimed to prepare a probe that does not change the functional response of the neutrophil, but allows for time-resolved imaging of these cells (i.e. inflammation) via FPR2/ALX (Figure 1). Furthermore, differentiation of compound luminescence from an autofluorescent background (which is hard to distinguish in traditional fluorophores) allows for visualisation of compound uptake patterns within the neutrophil in both its activated state (when prior stimulation has occurred using an inflammatory stimulus, tumor necrosis factor alpha [TNFα]) and in an un-activated state (using phosphate buffered saline [PBS] as a control). By complexing Gd(III) instead of Tb(III), we were also able to prepare a compound with r_1 relaxivity values of 6.9 $mM^{-1}s^{-1}$, which are increased compared to typical octadentate structures (where r1 = 3 – 5 $mM^{-1}s^{-1}$).[39] The Eu(III) analogue was constructed to enable the macrocyclic conformational equilibria to be investigated by ^{1}H-NMR spectroscopy and therefore provide insight into the twisted square antiprism (TSAP) to square antiprism (SAP) geometry ratios of the complex.

Results and discussion

Synthetic procedures

The FPR2/ALX targeting unit Quin C1 (**6**) was prepared according to modified procedures previously described[22] and obtained as a crystalline solid after purification by column chromatography (Figure 2 and 3). Compound **6** was further reacted with chloroacetyl chloride to produce **7**. Next, a DOTA-derived, macrocyclic scaffold was prepared following known protocols.[40,41,42] 1, 4, 7, 10-tetraazacyclododecane-1, 4, 7, 10-tetraacetic acid (DOTA)-derived macrocycles are commonly used for biomedical applications and their octadentate lanthanide coordination complexes are characterised by high kinetic inertness and thermodynamic stability under physiological conditions.[43] In brief, the mono-*tert*-butyloxycarbonyl protected compound **9** was prepared and reacted with chloroacetyl chloride, before combination with the *tert*-butyl protected 1, 4, 7, 10- tetraazacyclododecane-1, 4, 7-trisacetic acid (DO3A) macrocycle to yield **11**. Subsequent deprotection with trifluoroacetic acid and dichloromethane unmasked the amine terminal ligand scaffold **12** in high yields.

This journal is © The Royal Society of Chemistry 20xx

Please do not adjust margins

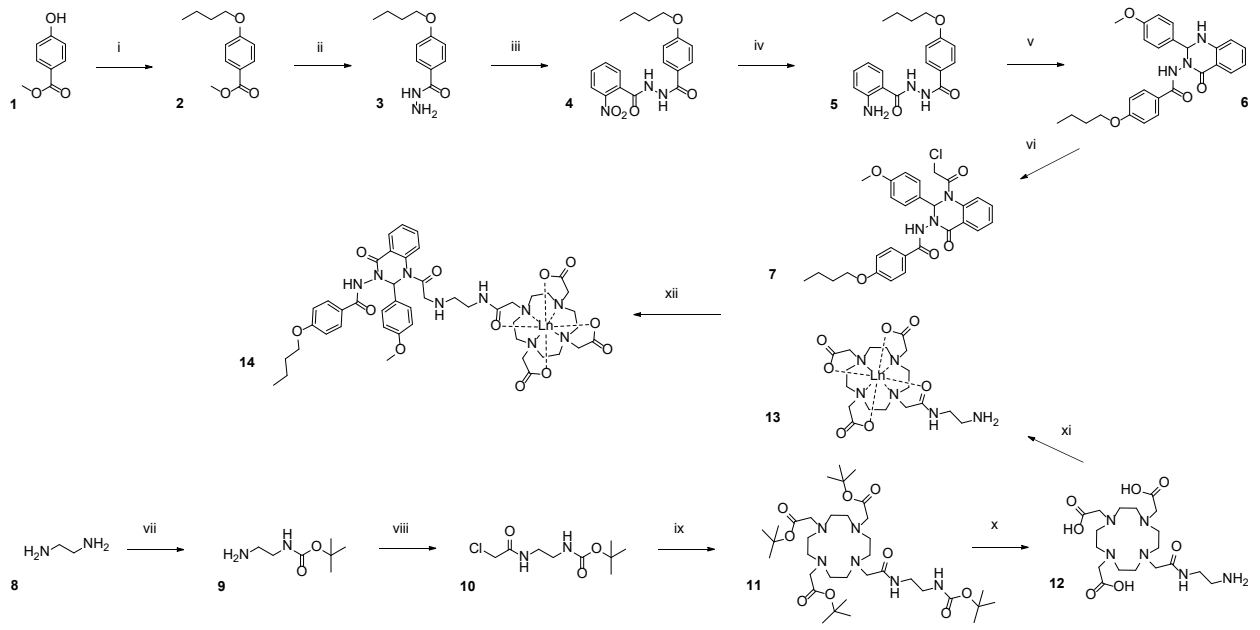

Figure 2: Synthetic pathway for preparation of the FPR2/ALX-targeted imaging probes. Reagents: i) 1-bromobutane, K_2CO_3, MeOH, ii) hydrazine monohydrate, EtOH, iii) 2-nitro-benzoyl chloride, K_2CO_3, DCM, iv) zinc dust, AcOH, DCM, v) 4-methoxy benzaldehyde, citric acid, EtOH, vi) chloroacetyl chloride, triethylamine, DCM, vii) di-tert-butyl dicarbonate, EtOH, viii) chloroacetyl chloride, triethylamine, DCM, ix) DO3A, K_2CO_3, MeCN, x) trifluoracetic acid, DCM, xi) Ln (Ln = Tb, Gd, Eu) trifluoromethane sulphonate, water pH 5.5, xii) K_2CO_3, MeCN.

Metal complexation was carried out using terbium or europium trifluoromethanesulfonate salts or gadolinium chloride hexahydrate in water at pH 5.5 to produce the lanthanide complexes Tb.**13**, Eu.**13** and Gd.**13**. The compounds were purified by dialysis using a 500-1000 Da molecular weight cut-off cellulose membrane, allowing separation of excess metal salts. Absence of free lanthanide ions was ascertained using the xylenol orange indicator test. To afford FPR2/ALX targeted lanthanide complexes, Tb.**13**, Eu.**13** and Gd.**13** were combined with the functionalised targeting moiety **7**. The resulting compounds Tb.**14**, Eu.**14** and Gd.**14** were isolated after Sephadex size exclusion chromatography, dissolved in a minimum amount of methanol and precipitated using diethyl ether.

Crystallography

The thus far unreported crystal structure of Quin C1 (**6**) was acquired by slow evaporation from methanol at room temperature and is depicted in Figure 3. The compound was found to crystallise as a mixture of both the *R* and *S* enantiomer (chiral carbon: C3), which stacked alternately. In the solid state, two twists within the molecule along the C3-C24 bond and the C12-C13 bond were observed, creating three planes. Bond lengths and angles are listed in the supplementary information. Intermolecular H-bonding between the O1 and H4A (on N4) atoms was observed with a bond distance calculated as 2.13 Å (Figure 3B).

Photophysical properties

Steady-state and time-gated luminescence and absorption spectra of Tb.**14** were recorded in aerated methanol solutions (Figure 4A). Excitation at 350 nm yielded an emission maximum at 441 nm. Two maxima at 227 nm and 347 nm (λ_{em}= 440 nm) were apparent within the excitation spectrum. Upon application of a 0.1 ms time gate and excitation at 350 nm,

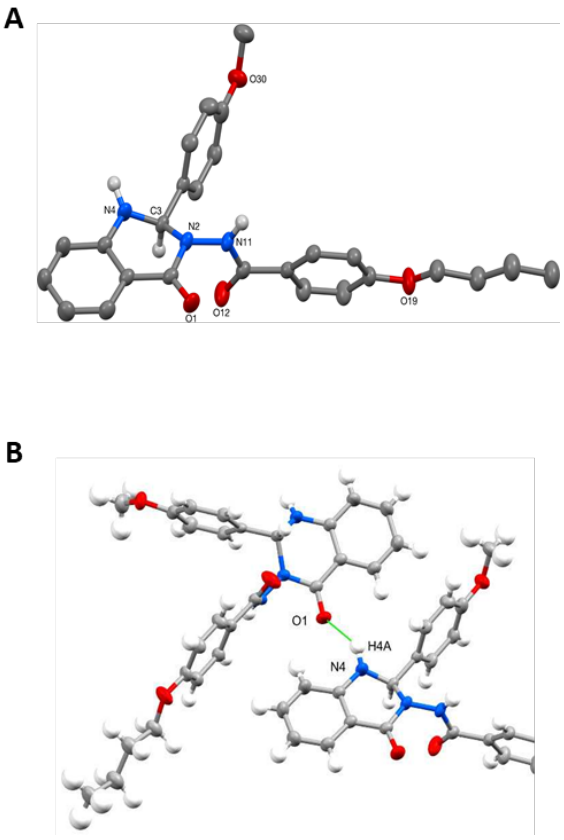

Figure 3: A) Crystal structure of **6** (50% probability ellipsoids) and B) excerpt of structure showing H-bonding interactions.

characteristic terbium emission bands with maxima at 490 nm, 546 nm, 586 nm and 620 nm arising from $^5D_4 \rightarrow {}^7F_J$ transitions, for J = 6, 5, 4 and 3 respectively were apparent within the spectrum, demonstrating sensitisation of the lanthanide via the ligand chromophore. Metal-centred luminescence lifetimes of Tb.**14** were recorded in water and deuterium oxide and their decays were fitted to a single-exponential function (Figure S1, ESI). The resulting values were determined as τ_{D2O} = 2.8 ms and τ_{H2O} = 1.9 ms. Using the empirical relationship between the lifetimes of a species in H_2O and D_2O and the number of bound water molecules respectively,[44,45] the hydration number (q-value) was determined as q = 0.8, suggesting an octadentate ligand environment and a 9-coordinate metal centre.

In order to assess the short-lived, ligand-based components of the emissio, Time-Correlated Single Photon counting (TCSPC) studies were undertaken on a PicoQuant FluoTime 300 equipped with a 375 nm picosecond pulsed laser. The resulting decay curves for short lifetimes were fitted using a numerical reconvolution algorithm to account for the finite Instrument Response Function (IRF) using FluoFit software. Interestingly, the fluorescence decay obtained for Tb.**14** by this method could not be fitted to a single exponential decay curve, but instead was best fitted to a biexponential decay with 2 components with ns range lifetimes of τ_1 = 11 ns (approximately 85% fractional intensity) and τ_2 = 3 ns (approximately 15% fractional intensity) (Figure S2, ESI). This phenomenon is tentatively assigned to dual emission occurring from two orthogonal components of the organic system, which is supported by the observation of two ligand-based emission processes in the complex (see below). The preferred non-planar conformation around the diacyl hydrazine linkage will prevent efficient relaxation through dipole-dipole interactions and preserve independent emission from each component (see Figure 3).

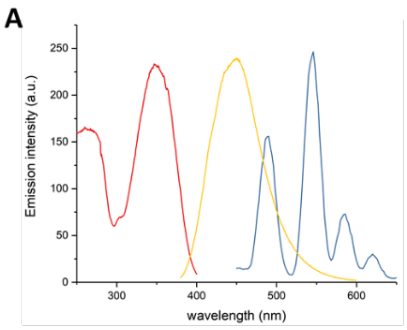

Figure 4: A) Excitation spectrum (red), steady state emission spectrum (yellow) and emission spectra with an applied time-gate of 0.1 ms (blue) of compound Tb.**14** in methanol B) emission spectra of Gd.**14** at room temperature (dark blue) and 77 K (light blue) in ethanol.

In the europium complex (Eu.**14**), weak lanthanide emission was observed upon application of a time gate, while steady state emission spectra were comparable to those of the terbium analogue (λ_{max} = 451 nm for emission and λ_{max} = 348 nm for the longest wavelength excitation band in methanol, Figure S3, ESI). The faint lanthanide-based emission is likely indicative of a poor energy match between the relevant excited state within the antenna unit and the $^5D_0$ europium emissive state.

Typically, population of the lanthanide excited state is known to proceed via an energy transfer process (sensitisation).[46] Often, this pathway occurs through ligand excitation, intersystem crossing to the ligand-based excited triplet state followed by an energy transfer to the relevant emissive lanthanide state.[47] Gadolinium-centred emission occurs within the UV range of the spectrum and thus does not interfere with the visible light ligand-based emission, making the gadolinium analogue (Gd.**14**) a convenient lanthanide complex model to study ligand-based emission.[48]

To observe phosphorescence ($T_1 \rightarrow S_0$) from the ligand triplet energy level (T_1) which is typically considered responsible for sensitising the metal unit, emission spectra of Gd.**14** under low temperature conditions were recorded (to minimise triplet state deactivation by non-radiative processes). The obtained spectra revealed that upon cooling to 77 K in ethanol, an intense transition at 416 nm and a weak maximum at 539 nm were apparent (Figure 4B). The weak, lower energy band was tentatively assigned to the ligand-centred triplet state, whereas the shift to higher energy emission at low temperature (441 nm at room temperature to 416 nm at 77 K) is indicative of a charge transfer process.[49] These results led us to hypothesise that the ligand-based emission seen at room temperature could result from a thermally activated ligand charge transfer band (supported by the broad, structureless nature of emission and absorption bands with large Stokes' shifts), while a shift to higher energies of that band are observed at low temperature. The data further led us to hypothesise that an unusual lanthanide sensitisation pathway in the terbium complex may occur via the energetically well-matched charge transfer band (at 22,575 cm^{-1} compared to the Tb(III) $^5D_4$ excited state at 20,400 cm^{-1}),[50] whereas the tentatively assigned ligand triplet state (at 18,553 cm^{-1}) appears too low in energy for terbium sensitisation. Additionally, our results suggest that neither the ligand triplet state nor the charge transfer state can efficiently sensitise europium emission (Figure S3, ESI).

Similar sensitisation pathways via an antenna charge transfer excited state have been studied extensively for Eu(III), Yb(III) and Nd(III) complexes,[51,52] whereas examples of intra ligand charge transfer (ILCT)-sensitised Tb(III) emission are rare.[49] This sensitisation pathway, which proceeds via the strong, ligand-

This journal is © The Royal Society of Chemistry 20xx

based absorption band that is typically associated with an ILCT state, could be harnessed for microscopy applications.

Investigation into conformational equilibria

Ln(III)-DOTA complexes form two well characterised stereoisomers that are visualised as a square antiprism (SAP) isomer and a twisted square antiprism (TSAP) isomer. The two isomers can interconvert in solution and differ in the twist angle between the oxygen and the nitrogen binding planes.[53,54] The equilibrium between the two species can be tuned by different factors[55,56,57] and is particularly relevant to gadolinium complexes with uses in MRI, as the TSAP geometry is often associated with substantially increased water exchange rates and correspondingly higher relaxivity values.[58,59]

Within the ^{1}H-NMR spectrum of Eu.**14** (Figure S4A, ESI) resonances consistent with the SAP axial proton region (29 - 35 ppm) and the minor TSAP isomer axial protons (between 10 and 14 ppm) were present.[60] The signals appear broadened compared to those observed in the starting material (Figure S4B, ESI) and more than four proton environments were observed, likely arising from further, superimposed conformational equilibria.[61] In addition, the spectrum suggests an increase in the amount of the minor TSAP isomer compared to the starting material (estimated prevalence by relative integration 0.36:1), consistent with previous reports that increasing steric demands on the lanthanide ion leads to an increased preference for the TSAP geometry.[57]

Relaxometric measurements

Next, the longitudinal relaxation time (T_1) of Gd.**14** in water was determined at distinct molar concentrations (at 400 MHz and 294 K) using inversion recovery experiments. The resulting relaxivity values were estimated according to a graphical procedure[62] and a value of 6.9 $mM^{-1}s^{-1}$ was measured for Gd.**14** in water. This value is surprisingly high, considering that low molecular weight, octadentate gadolinium chelates typically exhibit r_1 values of 3 – 5 $mM^{-1}s^{-1}$,[39] which may be driven by the observed increase in TSAP isomer compared to the starting material. Although used as an indication, this value does not predict how well the compound would perform in a more complicated *in vitro* or *in vivo* setting.

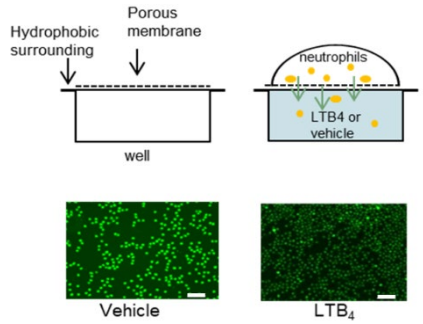

Figure 5: Schematic of chemotaxis assay showing how freshly isolated human neutrophils incubated with different concentrations of Tb.**14** were added to the top wells of a Neuroprobe chemotaxis chamber, whilst LTB_4 (10^{-6} M) was added to the bottom wells to assess whether the compound affects neutrophil chemotactic responses. Example images of migrated neutrophils are shown (scale bar = 100 µm).

***In vitro* viability assessment**

For Tb.**14** to provide a useful platform for imaging inflammation via FPR2/ALX, it is crucial to ensure the compound itself does not modify the normal immunological functions of neutrophils (such as their ability to move towards a chemical gradient, transmigrate through an endothelial layer and their granular content release e.g. myeloperoxidase [MPO]). With this in mind, neutrophils were pre-treated with saline control or varying, biologically relevant concentrations of the compound (10^{-6}, 10^{-7}, 10^{-8} and 10^{-9} M) and neutrophil functional responses were analysed using three distinct assays to assess chemotaxis, transmigration and MPO release (Figure 6). As the initial recruitment of neutrophils in inflammation is driven by their ability to move towards a chemical signal or chemoattractant (e.g. leukotriene B_4 [LTB_4]), we tested the effect of neutrophils to migrate towards LTB_4 (10^{-6} M) or PBS vehicle with and without pre-treatment with Tb.**14** (Figure 5). The data collected was expressed as a migration index (ratio of neutrophils

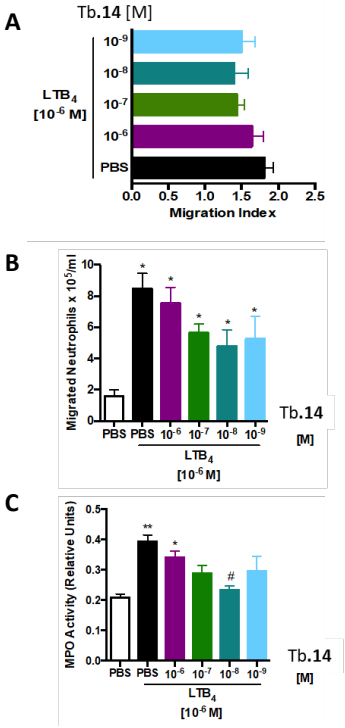

Figure 6: A) Chemotaxis data represented as migration index (calculated by dividing numbers of neutrophils migrated to LTB_4 by numbers of cells migrated to vehicle [phosphate buffered saline (PBS)]). B) Transmigration data expressed as the number of migrated neutrophils through an endothelial cell layer (human umbilical vein endothelial cells [HUVECs]) per unit volume in response to LTB_4 in presence of varying Tb.**14** concentrations or absence of the compound. C)) quantification of neutrophil myeloperoxidase (MPO) release upon stimulation using relative MPO activity compared to a standard. All data are mean ± SEM of 3-4 independent donors run in duplicate. *$p < 0.05$ vs. corresponding vehicle control group, $^{\#}p < 0.05$ vs. LTB_4 control group (Friedman and Dunn's test).

Please do not adjust margins

migrated in response to LTB_4 and neutrophils migrated in response to vehicle) and statistical analysis confirmed that at relevant compound concentrations, no significant change in neutrophil mobility was observed compared to the PBS control (Figure 6A).

An important part of the inflammatory response is the ability of neutrophils to extravasate from blood vessels to the site of tissue injury.[63] To simulate this biological function, neutrophils were incubated with PBS control or varying concentrations of Tb.**14** (10^{-6}, 10^{-7}, 10^{-8} and 10^{-9} M) and their ability to migrate through a HUVEC layer towards a chemoattractant (LTB_4) was assessed. Figure 6B shows that the compound did not modify the ability of neutrophils to transmigrate towards LTB_4 at any of the concentrations tested. Although there appeared to be a trend towards less neutrophils migrating towards LTB_4 when treated with the lower Tb.**14** concentrations (i.e. 10^{-7} to 10^{-9}M), this was not significant when compared to the LTB_4 control. Equally, all groups (i.e. the LTB_4 control group and all Tb.**14** concentrations tested) produced significant effects when compared with the PBS control group, authenticating the use of Tb.**14** as an imaging agent.

Under inflammatory conditions neutrophils release reactive species from their intracellular granules in order to eliminate invading pathogens. Amongst these granular proteins, myeloperoxidase (MPO, a marker of neutrophil activation) is known to perform anti-microbial functions as well as to contribute significantly to neutrophil dependent inflammation.[64] To test whether presence of Tb.**14** changes MPO production in activated neutrophils compared to the control, we assessed MPO activity in neutrophils that had transmigrated through an endothelial (HUVEC) layer. In this assay, we found a concentration dependent response of Tb.**14** on neutrophil MPO production. At high concentrations (10^{-6} M), Tb.**14** did not affect the ability of neutrophils to release their MPO, however, we found that an attenuation of granular release occurred at 10^{-8} M, whereas the presence of certain Tb.**14** concentrations (10^{-7} M and 10^{-9} M) produced little MPO effects. These results suggest that Tb.14 at a concentration of 10^{-6}M is more suitable as an imaging agent as this concentration does not inhibit the ability of neutrophils to release their MPO i.e. perform their immune response.

Proof of concept time-resolved microscopy investigation

Human neutrophils were isolated and pre-treated with vehicle (PBS) or stimulated with TNFα. Neutrophils were subsequently incubated with Tb.**14**, fixed and prepared for visualisation using a time-resolved confocal fluorescence microscope. To obtain terbium-based signals, emission was recorded as a lifetime map using pulsed 375 nm laser excitation.

At concentrations of 10^{-4} M to 10^{-6} M, no metal-based signals were observed. Upon increasing probe concentrations to 10^{-3} M, ring-like structures of pseudo-intensity on the cellular periphery were evident within the stimulated group, (Figure 7A), as were randomly speckled areas of increased signal. Within the stimulated group, presence of terbium-based signals were found, whereas no long-lived emission components were obtained in unstimulated samples (figure 7B). The overall averaged cellular decay times within the stimulated group of ~20 µs are short compared to lanthanide-only emission observed in a cuvette. However, it should be noted that these preliminary data were obtained using TCSPC methods including the entire range of emission lifetimes, rather than using time-gated methods to measure phosphorescence alone. Hence, the calculated average lifetimes in Fig. 7 include all cellular emission including autofluorescent background signals (typically sub 10 ns) and short-lived Quin C1-based emission. Although lanthanide complexes are typically less prone to quenching by cellular material than organic dyes due to the triplet nature of the emission, it is also possible that the cellular lifetime of the complex differs from the solution lifetime. However, while the average lifetime method does not demonstrate any ms component to the decay, the observed 20 µs average is a demonstration of uptake of the complex in stimulated cells being in the order of 10^3 x the average lifetime observed in unstimulated cells. The pattern of attachment observed in stimulated samples is consistent with images previously observed using fluorescently tagged peptides.[65] In the study, attachment to the FPRs in unstimulated neutrophils occurred uniformly distributed throughout the cell. In contrast, for stimulated neutrophils peptide-labelled receptors accumulated around the cell periphery or, in a further cell subset, in areas of receptor clusters.

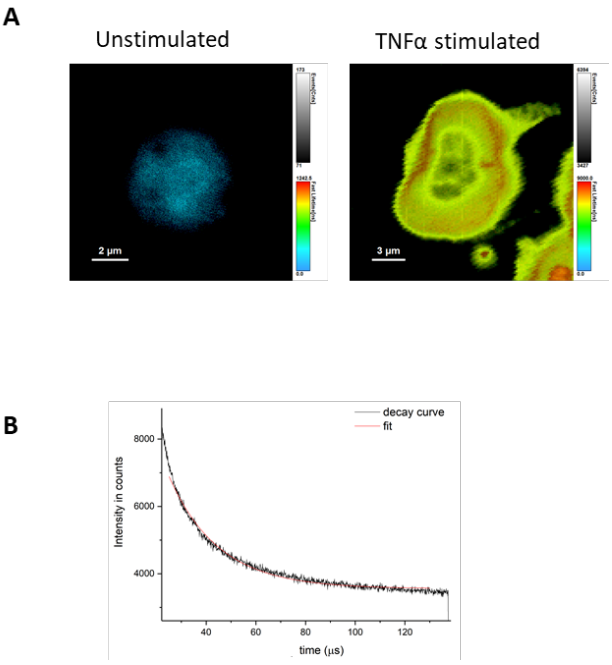

Figure 7: A) lifetime maps of neutrophils obtained using a time-resolved confocal microscope to visualise uptake of Tb.**14** in unstimulated cells or cells that had been treated with TNFα prior to incubation with the compound. Long-lived signals around the cell periphery indicate presence of the compound, while no long-lived decay components were detected in unstimulated samples. B) Luminescence lifetime decay and tail-fitting (shown in red) of the overall average decay in a stimulated neutrophil, demonstrating terbium-based emission and an average cell lifetime of ~20 µs.

This journal is © The Royal Society of Chemistry 20xx

Please do not adjust margins

Please do not adjust margins

Conclusions

Lanthanide frameworks tethered to a small-molecule FPR2/ALX ligand were described in this work and their ability to act as cellular imaging probes was investigated. The targeting moiety, Quin C1, was found to act as an efficient sensitising unit for terbium-emission, whereas the europium analogue appeared largely non-luminescent under time-gated conditions. Proton NMR spectroscopy of Eu.**14** revealed typical DOTA-type signals. Attachment of the targeting group was found to result in a relative increase of the TSAP isomer (and thus preferable water exchange properties), which was also reflected in the comparatively high r_1 value of 6.9 $mM^{-1}s^{-1}$ at 400 MHz and 294 K (compared to typical r_1 values of ~3-5 $mM^{-1}s^{-1}$ for commercially used contrast agents based on octadentate metal-binding frameworks). *In vitro* testing of compound Tb.**14** was conducted to examine the effects on neutrophil functional responses in physiological and pathological conditions. We ascertained that neutrophil functions remained intact at certain concentrations of Tb.**14**. Despite weak cellular signals, a time-resolved microscopy proof of concept experiment confirmed preferential uptake of Tb.**14** occurred in activated cells, and distinctive cellular morphologies were observed, whereas no observable long-lived signals were noted in unstimulated groups.

Experimental

Materials and general procedures

Reagents were bought from Sigma Aldrich or Fisher Scientific and used without further purification. Deuterated solvents were bought from Goss Scientific. ^{1}H-NMR and ^{13}C-NMR spectra were recorded on a Bruker AMX-500 spectrometer at room temperature unless stated otherwise. Coupling constants are quoted in Hertz (Hz) and multiplicities are abbreviated as: s = singlet, d = doublet, t = triplet, q = quartet, m = multiplet and br = broad. Electrospray Time-of- Flight and MALDI mass spectra were obtained using a Waters LCT Premier. Thin-layer chromatography was conducted using pre-coated Silica gel 60, F254 plates with a thickness of 0.2 nm. Column chromatography was performed using silica gel or Sephadex-G10 and laboratory grade solvents, under mild pressure.

Synthetic procedures

Compounds **2**, **3** ,**4** ,**5** and **6** were prepared as detailed below, using procedures that had been modified from reference.[22]

Methyl 4-butoxybenzoate (2)

Potassium carbonate (6.83 g, 50 mmol) and methyl 4-hydroxybenzoate (5.00 g, 33 mmol) were dissolved in methanol (60 mL) and stirred under nitrogen at 0°C for 20 minutes. 1-Bromobutane (4.97 g, 37 mmol) was added dropwise before the mixture was heated at reflux for 23 hours. The solvents were removed *in vacuo*, the reaction mixture was dissolved in dichloromethane (50 mL), washed with water (3 x 50 mL), brine (2 x 50 ml), dried over magnesium sulphate and concentrated. Purification was achieved by silica column chromatography in dichloromethane/petroleum ether (3:1) and yielded a clear oil (4.09 g, 60 %). ^{1}H-NMR (400 MHz, $CDCl_3$) δ_H (ppm): 0.99 (3H, t, $^3J_{HH}$ = 7.4 Hz), 1.51 (2H, m, $^3J_{HH}$ = 7.6 Hz), 1.80 (2H, m, $^3J_{HH}$ = 6.5 Hz), 3.89 (3H, s), 4.02 (2H, t, $^3J_{HH}$ = 6.5 Hz), 6.91 (2H, d, $^3J_{HH}$ = 8.9 Hz), 7.98 (2H, d, $^3J_{HH}$ = 8.9 Hz).
CI+: *m/z* 209 $\{M+H\}^+$, 226 $\{M+NH_4\}^+$.

4-Butoxybenzohydrazide (3)

Compound **2** (2.70 g, 13 mmol) and hydrazine monohydrate (2.60 g, 52 mmol) were dissolved in ethanol (50 mL) and heated at 65°C under a nitrogen atmosphere for 24 hours, before further 4 equivalents of hydrazine monohydrate were added. The reaction was heated for further 30 hours. Subsequently, the reaction mixture was concentrated *in vacuo* and the resulting oil was purified by activated alumina column chromatography (Brockman grade V), eluting initially with dichloromethane. Once the starting material had eluted, a methanol gradient (up to 20 %) was added to afford a crystalline white solid (1.90 g, 70 %). ^{1}H-NMR (400 MHz, $CDCl_3$) δ_H (ppm): 0.99 (3H, t, $^3J_{HH}$ = 7.4 Hz), 1.51 (2H, m, $^3J_{HH}$ = 7.6 Hz), 1.79 (2H, m, $^3J_{HH}$ = 6.5 Hz), 4.01 (2H, t, $^3J_{HH}$ = 6.5 Hz), 4.07 (2H, br, -N$\underline{H_2}$), 6.93 (2H, d, $^3J_{HH}$= 8.9 Hz, H_a), 7.70 (2H, d, $^3J_{HH}$ = 8.9 Hz, H_b). ES+: *m/z* 209 $\{M+H\}^+$

2-(4-Butoxybenzoyl)hydrazide 2-nitro-benzoic acid (4)

4-Butoxybenzohydrazine (1.80 g, 9 mmol) and potassium carbonate (1.20 g, 9 mmol) were dissolved in dichloromethane at 0°C under a nitrogen atmosphere. 2-Nitro-benzoyl chloride (1.0 mL, 7.8 mmol) was added slowly to the solution, which was gradually allowed to warm to room temperature. After stirring for further 15 hours, the reaction mixture was washed with water (2 x 50 mL) and brine (2 x 50 mL), the organic fractions were combined and dried over magnesium sulphate before the remaining solvents were removed *in vacuo* to yield a pale yellow solid (1.38 g, 43 %). ^{1}H-NMR (400 MHz, MeOD) δ_H (ppm): 1.01 (3H, t, $^3J_{HH}$ = 7.4 Hz), 1.53 (2H, m, $^3J_{HH}$ = 7.4 Hz), 1.80 (2H, m, $^3J_{HH}$ = 6.4 Hz), 4.07 (2H, t, $^3J_{HH}$ = 6.4 Hz), 7.01 (2H, d, $^3J_{HH}$ = 8.9), 7.72-8.16 (6H, br).
ES+: *m/z* 358 $\{M+H\}^+$

2-(4-Butoxybenzoyl)hydrazide 2-amino-benzoic acid (5)

Compound **4** (1.38 g, 3.8 mmol) was dissolved in a mixture of acetic acid and dichloromethane (1:1, 80 mL) at 0°C. Excess zinc dust (2.50 g, 38.4 mmol) was added to the stirring mixture which was subsequently gradually allowed to warm to room temperature. After 16 hours, the mixture was filtered through celite and washed with dichloromethane (10 x 20 mL). The solvents were removed *in vacuo*, before the reactants were dissolved in dichloromethane, washed with saturated sodium bicarbonate (3 x 50 mL) and dried over magnesium sulphate to yield an off-white solid (0.87 g, 70 %). ^{1}H-NMR (400 MHz, MeOD) δ_H (ppm): 1.01 (3H, t, $^3J_{HH}$ = 7.4 Hz), 1.54 (2H, m, $^3J_{HH}$ = 7.6 Hz), 1.79 (2H, m, $^3J_{HH}$ = 6.4 Hz), 4.07 (2H, t, $^3J_{HH}$ = 6.4 Hz), 6.75 (2H, m), 7.02 (2H, m), 7.32 (1H, m), 7.73 (1H, m), 7.90 (2H, m).
ES+: *m/z* 368 $\{M+MeCN\}^+$

Quin C1 (6)

Please do not adjust margins

Please do not adjust margins

2-(4-Butoxybenzoyl)hydrazide 2-amino-benzoic acid (0.54 g, 1.6 mmol) and 4-methoxy benzaldehyde (0.27 g, 2.0 mmol) were dissolved in ethanol (20 ml) and heated at reflux for an hour before addition of citric acid (0.38 g, 2.0 mmol). The reagents were further refluxed for 48 hours. Residual solvent was removed *in vacuo* and the reaction mixture was dissolved in dichloromethane and filtered. The filtrate was purified by silica column chromatography eluting with a dichloromethane and acetone gradient of 0 % - 50 % to yield a white solid (0.59 g, 83 %). ^{1}H-NMR (400 MHz, d6-acetone) δ_H (ppm): 0.95 (3H, t, $^3J_{HH}$ = 7.4 Hz), 1.47 (2H, m, $^3J_{HH}$ = 7.6 Hz), 1.74 (2H, m, $^3J_{HH}$ = 6.5 Hz), 3.78 (3H, s), 4.02 (2H, t, $^3J_{HH}$ = 6.5 Hz), 6.30 (2H, br), 6.83 (1H, td, $^3J_{ortho}$ = 7.1 Hz, $^4J_{meta}$ = 1.0 Hz), 6.90 (5H, m), 7.35 (1H, td, $^3J_{ortho}$ = 8.0 Hz, $^4J_{meta}$ = 1.6 Hz), 7.49 (2H, d, $^3J_{ortho}$ = 8.6), 7.66 (2H, m), 7.84 (1H, dd, $^3J_{ortho}$ = 7.8 Hz, $^4J_{meta}$ = 1.5 Hz), 9.38 (1H, br). ^{13}C-NMR (400 MHz, d6-acetone) δ_H (ppm): 14.1, 19.8, 31.9, 55.6, 68.5, 74.8, 114.4, 114.8, 115.5, 119.1, 129.3, 130.2, 130.4, 134.6, 149.7, 161.4, 162.9, 165.3, 166.3, 180.7.
HRMS: *m/z* calculated: 446.2080, found: 446.2089 for {M+H}$^+$

Quin C1-acetyl chloride (7)
Compound **6** (0.10 g, 0.22 mmol) and triethylamine (0.03 g, 0.33 mmol) were dissolved in dichloromethane (3 mL) under a nitrogen atmosphere. The stirring solution was immersed in an ice/acetone bath and chloroacetyl chloride (0.030 g, 0.26 mmol) in dichloromethane (2 mL) was added dropwise. The reaction mixture was gradually warmed to room temperature and stirred overnight, before it was washed with water (2 x 5 mL) and dried over magnesium sulphate. Purification was achieved by silica column chromatography eluting with a dichloromethane/acetone mixture (95:5) to afford an off-white solid (0.07 g, 60 %). ^{1}H-NMR (400 MHz, d6-acetone) δ_H (ppm): 0.97 (3H, t, $^3J_{HH}$ = 7.4 Hz), 1.50 (2H, m, $^3J_{HH}$ = 7.6 Hz), 1.78 (2H, m, $^3J_{HH}$ = 7.2 Hz), 3.72 (3H, s), 4.08 (2H, t, $^3J_{HH}$ = 6.5 Hz), 4.84 (2H, br), 6.81 (2H, dt, $^3J_{ortho}$ = 8.9 Hz, $^4J_{meta}$ = 2.1 Hz), 7.02 (2H, m), 7.13 (1H, br, s), 7.39 (3H, m), 7.58 (2H, m), 7.96 (3H, m), 10.37 (1H, br). ^{13}C-NMR (400 MHz, d6-acetone) δ_H (ppm): 13.1, 18.8, 30.9, 54.5, 67.6, 113.7, 114.1, 124.0, 126.4, 127.7, 128.5, 129.6, 132.9, 159.8, 160.4, 162.5, 165.7.
HRMS: *m/z* calculated: 552.1790, found: 552.1793 for {M+H}$^+$

N-(tert-butoxycarbonyl)-1,2-diaminoethane (**9**)[40], *N*-(tert-butoxycarbonyl)-N'-aminoacetylchloride (**10**)[41], 1,4,7-Tris(*tert*-butoxycarbonylmethyl)-10-(N-(2-tertbutoxycarbonylaminoethyl) acetamide)-1,4,7,10-tetraazacyclododecane (**11**)[42] and 1,4,7-Tris(carbonylmethyl)-10-(aminoethyl-N-acetyl)-1,4,7,10- tetraazacyclododecane (**12**)[42] were prepared as detailed in the respective references.

Preparation of Ln.13[42]
Compound **12** and the respective lanthanide salt were dissolved in water in a 1:1.1 molar ratio, the pH was adjusted to 5.5 and the solution was stirred overnight at room temperature. Subsequently, the pH of the mixture was adjusted to 10 using a sodium hydroxide solution (1 M) and stirred for 45 minutes. The suspension was centrifuged and filtered to remove inorganic solids. Next, the pH of the filtrate was readjusted to 7 using a hydrochloric acid solution (1 M) and a xylenol orange test was performed. Water was removed *in vacuo* and the residue was recrystallised from a methanol and diethyl ether mixture and repeatedly washed with diethyl ether. Tb.**13:** (0.05 g, 59 %). IR (solid) in cm^{-1}: 3472, 2359, 1599, 1438, 1406, 1256, 1168, 1036. HRMS: *m/z* calculated: 603.1575 found: 603.1580 for {M+H}$^+$. Eu.**13:** (0.21 g, 88 %). ^{1}H-NMR (400 MHz, D_2O) δ_H (ppm): -16.66, -16.20, -15.60, -14.97, 14.67, -14.19, -13.91, -12.60, -11.58, -10.91, -9.41, -8.47 to -6.95, -6.68, -5.53, -5.02, -4.25, -3.24, -2.31, -1.72, -1.03, -0.45, 0.38, 1.17, 1.48, 2.49, 2.81 – 4.51, 6.78, 10.53, 11.30, 11.77 – 12.85, 13.52, 30.74, 31.88, 33.70, 34.07. HRMS: m/z calculated: 595.1531 found: 595.1548 for {M+H}$^+$. Gd.**13:** (0.05 g, 35 %). HRMS: m/z calculated: 602.1574, found: 602.1576 for {M+H}$^+$

Preparation of Ln.14
Potassium carbonate and Ln**.13** (in 5:1 molar ratios) were suspended in acetonitrile and stirred for half an hour before addition of **7** (1 equivalent). The mixture was heated at 60°C for two days. Inorganic salts were removed by filtration and residual solvents were evaporated to yield a white solid. The crude product was isolated by Sephadex G-10 size exclusion chromatography eluting with MilliQ water. Tb.**14:** (0.02 g, 25 %). IR (solid) in cm^{-1}: 2361, 1607, 1251, 1173. HRMS: *m/z* calculated: 1089.4792, found: 1089.4794 for {M+H}$^+$. Eu.**14:** ^{1}H-NMR (400 MHz, D_2O) δ_H (ppm): -17.17 to -15.97, -15.76, -13.40, -12.79 to -10.07, -9.37, -8.25 to-6.79, -6.59, -5.38, -4.85, -3.28, -2.59 to -1.77, -1.00, -0.45, 0.51, 0.96, 1.26, 1.48, 1.79, 1.91, 2.09, 2.69, 3.52-4.27, 5.89, 5.94, 5.99, 6.72-8.55, 10.92-14.33, 29.55-34.30. HRMS: *m/z* found: 1182.5885 for {M+H_2O+2 MeCN+H}$^+$. Gd.**14:** (0.02 g, 30 %). HRMS *m/z*: calculated: 1087.3524, found: 1087.3661 for {M+H}$^+$

X-ray crystal structure of 6
Crystal data for **6**: $C_{26}H_{27}N_3O_4$, *M* = 445.50, monoclinic, $P2_1/c$ (no. 14), *a* = 14.1692(8), *b* = 13.5603(6), *c* = 12.7578(7) Å, β = 110.407(7)°, *V* = 2297.4(2) Å^3, *Z* = 4, D_c = 1.288 g cm^{-3}, μ(Mo-Kα) = 0.088 mm^{-1}, *T* = 173 K, colourless tabular needles, Agilent Xcalibur 3 E diffractometer; 4582 independent measured reflections (R_{int} = 0.0174), F^2 refinement,[66,67] R_1(obs) = 0.0527, wR_2(all) = 0.1405, 3195 independent observed absorption-corrected reflections [$|F_o| > 4\sigma(|F_o|)$, completeness to θ_{full}(25.2°) = 98.8%], 316 parameters. CCDC 1945848.
The C3-bound *p*-methoxyphenyl group, as well as C3 itself, in the structure of **6** was found to be disordered. Two orientations were identified of *ca*. 73 and 27% occupancy, their geometries were optimised, the thermal parameters of adjacent atoms were restrained to be similar, and only the non-hydrogen atoms of the major occupancy orientation were refined anisotropically (those of the minor occupancy orientation were refined isotropically). As a consequence of this disorder the N4–H hydrogen atom was also disordered across two sites, and so rather than being found from a Δ*F* map the two orientations were added in idealised positions with riding thermal parameters. The N11–H hydrogen atom, by contrast, was located from a Δ*F* map and refined freely subject to an N–H distance constraint of 0.90 Å.

 This journal is © The Royal Society of Chemistry 20xx

Please do not adjust margins

Please do not adjust margins

Photophysical measurements

UV-vis absorption spectra were recorded on a Perkin Elmer 650 spectrometer in quartz cuvettes. Concentrations were adapted to ensure a sensible absorbance range. Fluorescence excitation and emission spectra were obtained using a Varian Cary Eclipse spectrophotometer.

Lanthanide-based lifetimes were measured using a Varian Cary Eclipse spectrophotometer in the phosphorescence mode, using 1 mM solutions in water or deuterium oxide. The integrated intensity was recorded after excitation of the samples at 350 nm. The gate time was fixed at 0.1 ms with both excitation and emission slits set at 20 nm. The resulting decay curves were fitted to a single exponential decay in Microsoft Excel. Hydration number (q-values) were calculated according to the following equation.[45]

$$q = A(\tau_{H2O}{}^{-1} - \tau_{D2O}{}^{-1} - B)$$

with A = 5 ms and B = 0.06 ms^{-1} for terbium.[68]

Short-lived organic component luminescence lifetimes were assessed in methanol solutions on a time resolved PicoQuant FluoTime 300 with a 375 nm picosecond pulsed laser using TCSPC. Fitting of the luminescence decay was conducted in FluoFit software.

Relaxometric measurements

Gd(III) complexes were dissolved in water at 3 different molar concentrations. The three solutions and a water standard were added into a glass capillary of 1.7 mm diameter, sealed and inserted into an NMR tube containing D_2O. Concentrations of Gd(III) present were assessed by measuring the difference in solvent shifts according to the magnetic susceptibility measurements conducted using the Evans method.[69] T_1 measurements were carried out using a Bruker Advance 400 spectrometer and inversion recovery measurements. Relaxivity values were calculated from the samples using a graphical procedure as described in the literature.[62] The longitudinal relaxation time (T_1) of Gd**.14** in water was determined at three distinct molar concentrations on a 400 MHz NMR spectrometer at 294 K. In addition, T_1 for just water ($T_{1,0}$) was determined under equivalent conditions.

Cellular studies

All *in vitro* studies were performed at LSU Health Sciences Center, Shreveport.

Neutrophil isolation

Blood samples were collected by healthcare professionals from healthy volunteers after obtaining informed consent (50 mL). The study was approved by the institutional review board of the LSUHSC-S (STUDY00000261) and conducted in accordance with the Declaration of Helsinki. After discarding approximately the first 3 mL (to avoid thrombin contamination), 45 mL of the sample were mixed with anticoagulant citrate dextrose (ACD) solution (5 mL). The samples were centrifuged (800 rpm for 20 minutes at room temperature) and the upper layer of plasma was removed before adding 1 x PBS (10 mL). Subsequently, 6% dextran (v/w, 1.8g in 30 mL 1x PBS) solution (8 mL) was added, the sample was gently inverted several times and left to sediment for 15 minutes. The leukocyte layer was collected and separated over a Histopaque 1077 gradient (10 mL per tube). After centrifugation (1500 rpm for 30 minutes at room temperature), the supernatant was removed. Cold water (9 mL) was added in order to lyse residual red blood cell, and subsequently mixed with 10 x PBS (1 mL). The volume was made up to 40 mL using 1 x PBS and centrifuged (1000 rpm for 10 minutes at room temperature). The supernatant was removed, and the cells were resuspended in 1 x PBS (5 mL) and the procedure was repeated. Finally, neutrophils were resuspended DMEM with 3% FCS (10 mL). The cells were counted using a Neubauer hemocytometer (diluted 1:1 with trypan blue) and the resulting cell count was diluted respectively for the number of cells required per assay performed.

Chemotaxis assay

Chemotaxis assays were run using 3 µm pore size ChemoTx® System 96 well plates (Neuro Probe, USA). LTB_4 (10^{-6} M, 29 µL, Sigma Aldrich) as a chemotactic stimulus or PBS as a control (29 µL) were added to the bottom of the wells. Freshly isolated neutrophils at a concentration of 4 x 10^6 cells/mL in DMEM and 3% fetal calf serum (FCS) were treated with vehicle (PBS) or varying concentrations of the compound for 10 minutes prior to addition to the top of the well plate membranes (25 µL). The plates were incubated for 3 hours at 37°C with 5% CO_2 before removal of the membrane. Migrated cells were manually counted using a Neubauer hemocytometer after dilution in a 1:1 ratio with trypan blue.

Transmigration assay

To assess cellular transmigration, 24-well plate inserts were treated with fibronectin for 30 minutes, before a monolayer of human umbilical vein endothelial cells (HUVECs, 32,000 cell/200 µL) were grown for 72 hours. HUVEC media was removed and neutrophils (10^6 cells/mL in DMEM and 3% FCS) that had been pre-treated with vehicle or varying compound concentrations for 10 minutes, were added to the inserts (500 µL). PBS (vehicle, 500 µL) or LTB4 (10^{-6} M, 500 µL) were added into a fresh 24-well plate set up and the inserts were transferred before incubation (3 hours at 37°C with 5% CO_2). Migrated cells were manually counted as described above.

Myeloperoxidase assay

Myeloperoxidase (MPO) release was quantified from cells that had been pre-activated by the transmigration assay. In order to achieve this, the neutrophil supernatant (20 µL) was collected from the bottom of transmigration plates and mixed in a 4:1 ratio with a 9:1:0.1 mixture of solutions A, B and C respectively that had been previously prepared. Solution A was made up of 5.4 g KH_2PO_4, 1.875 g EDTA and 5 mL Triton X-100. Solution B was a solution of 3,3',5,5'- tetramethylbenzidine (TMB, 10 mM) in acetone (2 mL) and solution C was an aqueous solution of hydrogen peroxide (30%, 25 µL) in water (10 mL). The cellular mixture was incubated at room temperature for approximately

Please do not adjust margins

Please do not adjust margins

5 minutes until a colour change occurred and the reaction was terminated by addition H_2SO_4 (1 M, 25 µL). Absorbance was read at 450 nm relative to a standard.

Time-resolved microscopy

Neutrophils were pre-treated with TNFα (50 ng/mL, 30 minutes) or with PBS (control) and incubated with varying concentrations of compound or vehicle for 45 minutes (37 ^{0}C, 5 % CO_2). Cells were seeded on poly-L-lysine sheets (300,000 cells per sheet) and fixed using paraformaldehyde (20 minutes) followed by direct transfer onto Fluoromont G coated glass slides. The sheets were firmly adhered to the slides using a nail base coat. Visualisation was performed on a MicroTime 200 (PicoQuant) time resolved confocal fluorescence microscopy system consisting of an Olympus IX73 confocal microscope fitted with a x100 oil objective excited with a picosecond pulsed 375 nm laser and coupled to a TimeHarp SPAD TCSPC unit. The single pixel decay profiles were analysed using the SymphoTime 64 software package.

Conflicts of interest

There are no conflicts to declare.

Acknowledgements

This work was supported by the UK Engineering and Physical Sciences Research Council (EPRSC) grant number EP/L016737/1. Dr F.N.E. Gavins acknowledges the support of the Royal Society Wolfson Fellowship under grant number RSWF/R3/183001.

Notes and references

1 P. Iribarren, J. Hu, Y. Le and J. M. Wang, *Immunol. Res.*, 2005, **1**, 165–176.
2 R. Jin, G. Yang and G. Li, *J. Leukoc. Biol.*, 2010, **87**, 779–789.
3 D. C. Rees, T. N. Williams and M. T. Gladwin, *Lancet*, 2010, **376**, 2018–2031.
4 S. I. Grivennikov, F. R. Greten and M. Karin, *Cell*, 2010, **140**, 883–899.
5 F. N. E. Gavins, *Trends Pharmacol. Sci.*, 2010, **31**, 266–276.
6 C. N. Serhan and P. M. Murphy, *Pharmacol. Rev.*, 2009, **61**, 119–161.
7 J. G. Filep, M. Sekheri and D. El, *Eur. J. Pharmacol.*, 2018, **833**, 339–348.
8 Y. Le, P. M. Murphy and J. M. Wang, *Trends Immunol.*, 2002, **23**, 541–548.
9 C. Dahlgren, M. Gabl, A. Holdfeldt, M. Winther and H. Forsman, *Biochem. Pharmacol.*, 2016, **114**, 22–39.
10 S. A. Vital, F. Becker, P. M. Holloway, J. Russell, M. Perretti, D. N. Granger and F. N. E. Gavins, *Circulation*, 2016, **133**, 2169–2179.
11 D. A. Dorward, C. D. Lucas, G. B. Chapman, C. Haslett, K. Dhaliwal and A. G. Rossi, *Am. J. Pathol.*, 2015, **185**, 1172–1184.
12 G. J. Stasiuk, H. Smith, M. Wylezinska-Arridge, J. L. Tremoleda, W. Trigg, S. K. Luthra, V. Morrison Iveson, F. N. E. Gavins and N. J. Long, *Chem. Commun.*, 2013, **49**, 564–566.
13 L. W. Locke, M. D. Chordia, Y. Zhang, B. Kundu, D. Kennedy, J. Landseadel, L. Xiao, K. D. Fairchild, S. S. Berr, J. Linden and D. Pan, *J. Nucl. Med.*, 2009, **50**, 790–798.
14 L. Xiao, Y. Zhang, Z. Liu, M. Yang, L. Pu and D. Pan, *Bioorg. Med. Chem. Lett.*, 2010, **20**, 3515–3517.
15 Y. Zhang, L. Xiao, M. D. Chordia, L. W. Locke, M. B. Williams and S. S. Berr, *Bioconjug. Chem.*, 2010, **21**, 1788–1793.
16 G. J. Stasiuk, P. M. Holloway, C. Rivas, W. Trigg, S. K. Luthra, M. Iveson, N. E. Gavins and N. J. Long, *Dalt. Trans.*, 2015, **44**, 4986–4993.
17 J. Pellico, A. V Lechuga-vieco, E. Almarza, A. Hidalgo, C. Mesa, I. Fernández-Barahona, J. A. Quintana, J. Bueren, J. A. Enriquez, J. Ruiz-Cabello and F. Herranz, *Sci. Reports*, 2017, **7**, 13242.
18 J. W. Babich, R. G. Tompkins, W. Graham, S. A. Barrow and A. J. Fischman, *J. Nucl. Med.*, 1997, **38**, 1316–1320.
19 K. A. Stephenson, J. Zubieta, S. R. Banerjee, M. K. Levadala, L. Taggart, L. Ryan, N. McFarlane, D. R. Boreham, K. P. Maresca, J. W. Babich and J. F. Valliant, *Bioconjug. Chem.*, 2004, **15**, 128–136.
20 K. A. Stephenson, S. R. Banerjee, T. Besanger, O. O. Sogbein, M. K. Levadala, N. Mcfarlane, J. A. Lemon, D. R. Boreham, K. P. Maresca, J. D. Brennan, J. W. Babich, J. Zubieta and J. F. Valliant, *J. Am. Chem. Soc.*, 2004, **126**, 8598–8599.
21 T. M. Stepniewski and S. Filipek, *Bioorganic Med. Chem.*, 2015, **23**, 4072–4081.
22 M. Nanamori, X. Cheng, J. Mei, H. Sang, Y. Xuan, C. Zhou, M. Wang and R. D. Ye, *Mol. Pharmacol.*, 2004, **66**, 1213–1222.
23 M. He, N. Cheng, W. Gao, M. Zhang, Y. Zhang, R. D. Ye and M. Wang, *Acta Pharmacol. Sin.*, 2011, **32**, 601–610.
24 N. J. Long and W. T. Wong, *The Chemistry of Molecular Imaging*, Wiley, 2015.
25 H. Kobayashi, M. Ogawa, R. Alford, P. L. Choyke and Y. Urano, *Chem. Rev.*, 2010, **110**, 2620–2640.
26 N. C. Shaner, P. A. Steinbach and R. Y. Tsien, *Nat. Methods*, 2005, **2**, 905–909.
27 S. X. Fang and P. R. Chen, *Chem. Commun.*, 2014, **50**, 14724–14727.
28 W. Becker, A. Bergmann, M. A. Hink, K. König, K. Benndorf and C. Biskup, *Microsc. Res. Tech.*, 2004, **63**, 58–66.
29 M. Rajendran and L. W. Miller, *Biophys. J.*, 2015, **109**, 240–248.
30 W. Wang, K. Vellaisamy, G. Li, C. Wu, C.-N. Ko, C.-H. Leung and D.-L. Ma, *Anal. Chem.*, 2017, **89**, 11679–11684.
31 C. Liu, C. Yang, L. Lu, W. Wang, W. Tan, C.-H. Leung and D.-L. Ma, *Chem. Commun.*, 2017, **53**, 2822–2825.
32 Z. Mao, M. Wang, J. Liu, L.-J. Liu, S. M.-Y. Lee, C.-H. Leung and D.-L. Ma, *Chem. Commun.*, 2016, **52**, 4450–4453.
33 J. Liu, C. Yang, C.-N. Ko, V. Kasipandi, B. Yang, M.-Y. Lee, C.-H. Leung and D.-L. Ma, *Sensors Actuators B*, 2017, **243**,

 This journal is © The Royal Society of Chemistry 20xx

Please do not adjust margins

Please do not adjust margins

971–976.
34 A. J. Amoroso and S. J. A. Pope, *Chem. Soc. Rev.*, 2015, **44**, 4723–4742.
35 C. P. Montgomery, B. S. Murray, E. J. New, R. Pal and D. Parker, *Acc. Chem. Res.*, 2009, **42**, 925–937.
36 M. Pan, W. Liao, S. Yin, S. Sun and C. Su, *Chem. Rev.*, 2018, **118**, 8889–8935.
37 M. Pan, B. Du, Y. Zhu, M. Yue, Z. Wei and C.-Y. Su, *Chem. A Eur. J.*, 2016, **22**, 2440–2451.
38 K. Vellaisamy, G. Li, W. Wang, C. Leung and D. Ma, *Chem. Sci.*, 2018, **9**, 8171–8177.
39 C. Yang and K. Chuang, *Med. Chem. Commun.*, 2012, **3**, 552–565.
40 W. Jiang, Q. Fu, H. Fan and W. Wang, *Chem. Commun.*, 2007, 259–261.
41 A. Fanning, S. E. Plush and T. Gunnlaugsson, *Chem. Commun.*, 2006, 3791–3793.
42 W. S. Perry, S. J. A. Pope, B. J. Coe, M. Kenwright and S. Faulkner, *Dalt. Trans.*, 2010, **39**, 10974–10983.
43 A. D. Sherry, P. Caravan and R. E. Lenkinski, *J. Magn. Reson. Imaging*, 2009, **1248**, 1240–1248.
44 W. D. J. Horrocks and D. R. Sudnick, *Acc. Chem. Res.*, 1981, **14**, 384–392.
45 A. Beeby, I. M. Clarkson, R. S. Dickins, S. Faulkner, D. Parker, L. Royle, A. S. de Sousa, J. a. G. Williams and M. Woods, *J. Chem. Soc. Perkin Trans. 2*, 1999, **2**, 493–504.
46 J.-C. G. Bünzli, *Coord. Chem. Rev.*, 2015, **293–294**, 19–47.
47 J.-C. G. Bünzli and S. V. Eliseeva, *Springer Ser. Fluoresc.*, 2011, **13**, 311–337.
48 M. Shi, F. Li, T. Yi, D. Zhang, H. Hu, C. Huang, V. Ad, F. U. V and N. U. V, *Inorg. Chem.*, 2005, **44**, 8929–8936.
49 A. D. Aléo, F. Pointillart, L. Ouahab, C. Andraud and O. Maury, *Coord. Chem. Rev.*, 2012, **256**, 1604–1620.
50 A. J. Amoroso and S. J. A. Pope, *Chem. Soc. Rev.*, 2015, **44**, 4723–4742.
51 W. Lo, W. Wong and G. Law, *RSC Adv.*, 2016, **6**, 74100–74109.
52 Z. Zhang, Y. Zhou, H. Li, T. Gao and P. Yan, *Dalt. Trans.*, 2019, **48**, 4026–4034.
53 M. Meyer, V. Dahaoui-Gindrey, C. Lecomte and R. Guilard, *Coord. Chem. Rev.*, 1998, **178–180**, 1313–1405.
54 S. Aime, M. Botta, M. Fasano, M. P. M. Marques, C. F. G. C. Geraldes, D. Pubanz and A. E. Merbach, *Inorg. Chem.*, 1997, **36**, 2059–2068.
55 I. J. F. Desreux, *Inorg. Chem.*, 1980, **19**, 1319–1324.
56 S. Aime, M. Botta and G. Ermondi, *Inorg. Chem.*, 1992, **19**, 4291–4299.
57 G. Tircso, B. C. Webber, B. E. Kucera, V. G. Young and M. Woods, *Inorg. Chem.*, 2011, **50**, 7966–7979.
58 A. C. L. Opina, M. Strickland, Y.-S. Lee, N. Tjandra, R. A. Byrd, R. E. Swenson and O. Vasalatiy, *Dalt. Trans.*, 2016, **45**, 4673–4687.
59 L. Dai, C. M. Jones, W. T. K. Chan, T. A. Pham, X. Ling, E. M. Gale, N. J. Rotile, W. C. S. Tai, C. J. Anderson, P. Caravan and G. L. Law, *Nat. Commun.*, 2018, **9**, 1–10.
60 D. Delli Castelli, M. C. Caligara, M. Botta, E. Terreno and S. Aime, *Inorg. Chem.*, 2013, **52**, 7130–7138.
61 J. Blahut, P. Hermann, Z. Tošner and C. Platas-Iglesias, *Phys. Chem. Chem. Phys.*, 2017, **19**, 26662–26671.
62 M. Rohrer, H. Bauer, J. Mintorovitch, M. Requardt and H. Weinmann, *Invest. Radiol.*, 2005, **40**, 715–724.
63 K. Ley, C. Laudanna, M. I. Cybulsky and S. Nourshargh, *Nat. Rev. Immunol.*, 2007, **7**, 678– 689.
64 Y. Aratani, *Arch. Biochem. Biophys.*, 2018, **640**, 47–52.
65 V. M. Loitto, B. Rasmusson and K. E. Magnusson, *J. Leukoc. Biol.*, 2001, **69**, 762–71.
66 G. M. Sheldrick, *SHELXTL, version 5, Bruker AXS Inc., Madison, Wisconsin, USA*.
67 G. M. Sheldrick, *Acta Crystallogr. Sect. C*, 2015, **71**, 3–8.
68 A. Beeby, I. M. Clarkson, R. S. Dickins, S. Faulkner, D. Parker, L. Royle, A. S. de Sousa, J. A. G. Williams and M. Woods, *J. Chem. Soc. Perkin Trans. 2*, 1999, **2**, 493–504.
69 D. M. Corsi, C. Platas-Iglesias, H. Van Bekkum and J. A. Peters, *Magn. Reson. Chem.*, 2001, **39**, 723–726.

Please do not adjust margins